Numerical Simulation of Dynamic Contact Angles and Contact Lines in Multiphase Flows using Level Set Method

by

Premchand Pendota

A Thesis Presented in Partial Fulfillment
of the Requirements for the Degree
Master of Science

Approved July 2015 by the
Graduate Supervisory Committee:

Marcus Herrmann, Chair
Konrad Rykaczewski
Kangping Chen

ARIZONA STATE UNIVERSITY

August 2015

ABSTRACT

Many physical phenomena and industrial applications involve multiphase fluid flows and hence it is of high importance to be able to simulate various aspects of these flows accurately. The Dynamic Contact Angles (DCA) and the contact lines at the wall boundaries are a couple of such important aspects. In the past few decades, many mathematical models were developed for predicting the contact angles of the interface with the wall boundary under various flow conditions. These models are used to incorporate the physics of DCA and contact line motion in numerical simulations using various interface capturing/tracking techniques. In the current thesis, a simple approach to incorporate the static and dynamic contact angle boundary conditions using the level set method is developed and implemented in multiphase CFD codes, LIT (Level set Interface Tracking) (Herrmann (2008)) and NGA (flow solver) (Desjardins *et al.* (2008)). Various DCA models and associated boundary conditions are reviewed. In addition, numerical aspects such as the occurrence of a stress singularity at the contact lines and grid convergence of macroscopic interface shape are dealt with in the context of the level set approach.

ACKNOWLEDGEMENTS

I would like to thank my adviser Dr. Marcus Herrmann for consistently supporting me in understanding various technical concepts and inspiring me to be more productive. I would also like to thank Dr. Konrad Rykaczewski for providing some insights into experimental aspects of this work and a few experimental images (Figure 1.1) presented in this thesis. I also thank Dr. Kangping Chen for serving as a committee member and helping me learn various concepts used in this work through his Continuum Mechanics course. I thank Carlos Ballesteros and Zechariah Jibben for proofreading the draft and providing invaluable suggestions. I am fortunate to have worked with very talented students at ASU Multiphase Research Lab who helped me on numerous occasions.Finally, I would like to thank my parents for supporting my education.

TABLE OF CONTENTS

LIST OF FIGURES

Figure | Page

Chapter 1

INTRODUCTION

1.1 Motivation

Multiphase flows can be found in many natural processes and industrial applications. Some examples for flows found in nature include rain drops falling through the atmosphere, gas bubbles in water, free surface flows and dust particles floating in the air. Multiphase flows also have numerous industrial applications such as, flow through porous media, atomizers, combustion, transport of dispersed solid particles in fluids and liquid sprays are a few of many applications.

Different phases in multiphase flows are separated by an interface, which is a physical and mathematical discontinuity on the continuum scale, as the physical properties of the fluid system change suddenly across the interface. In most of these applications, tracking the deformation or motion of the interface is of high interest; and there are several approaches available to understand the same, which are discussed in the succeeding chapters. When the interface touches the wall boundaries of the flow domain, a contact angle is formed between the wall boundary and the interface. The region common to the interface and the wall is called the Contact Line (CL) (contact point in a two – dimensional (2D) model). Fig. 1.1 shows different Contact Angles (CA) observed experimentally for different surface and liquid properties.

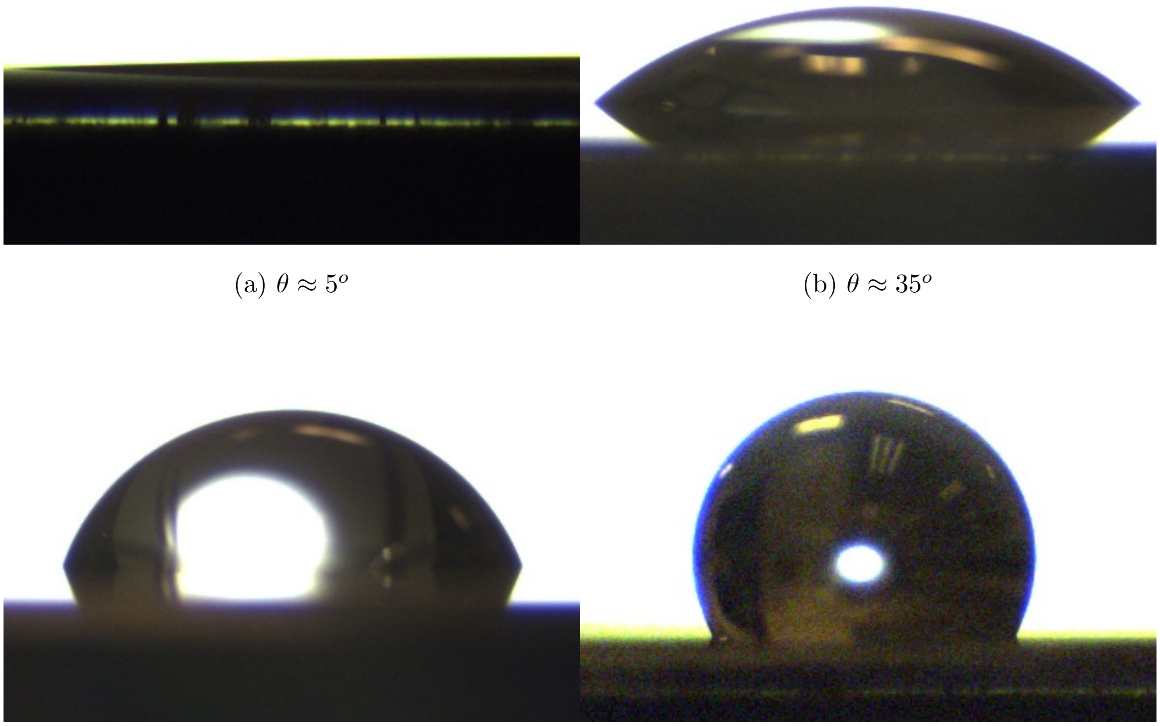

(a) $\theta \approx 5^o$ (b) $\theta \approx 35^o$

(c) $\theta \approx 65^o$ (d) $\theta \approx 110^o$

Figure 1.1: Experimentally observed contact angles. [1]

The CA is an important physical parameter which affects the macroscopic flow behavior to a great extent especially in low Reynolds number (Re) flows and capillary flows. Its value depends on various parameters including wall surface properties, the capillary number (Ca) of the flow near the contact line and the fluid properties. For instance, motion of a water droplet on a hydrophilic and a hydrophobic surface is very different because these surfaces result in different CA values. Another example which illustrates the importance of the contact angle is droplets pinching off from a condenser wall. The surface properties of the condenser walls can be changed to regulate

[1]Images provided by Dr. Konrad Rykaczewski.

the pinch–off process of the droplets (Walpot *et al.* (2007)) to improve the efficiency of the condenser. Thus, Computational Fluid Dynamic (CFD) studies involving such problems should incorporate the CA physics accurately to obtain physically valid results. In further sections, it is shown that the CA value which is prescribed as a Boundary Condition (BC) does impact the macroscopic interface shape to a great extent, in the numerical simulation of multiphase flows.

1.2 Thesis outline

The objective of the current work is to incorporate the physics of the CA and CL in multiphase CFD simulations using the Level Set Method (LSM). The resulting methods are added to the LIT (Level set Interface Tracking) (Herrmann (2008)) and NGA (flow solver) (Desjardins *et al.* (2008)) codes. First, a procedure to prescribe a given CA as a level set method boundary condition is developed. Some test cases which can be used to verify if the approach results in a correct contact angle treatment are presented. Then, the existing DCA models are reviewed and the ones which are most widely used are incorporated in LIT and NGA. In addition to prescribing the CA, grid convergence of interface profiles is studied and some modifications with physical basis are made to the BCs of the flow solver, in order to achieve the same.

Chapter 2

GOVERNING PHYSICS

2.1 Multiphase flow governing equations.

In this section the governing equations of two – phase flows, which are solved using the CFD codes are presented. The governing equations for an unsteady, incompressible, immiscible two phase fluid systems in vectorial notations are as follows:

1. Conservation of mass

$$\bigtriangledown \cdot \mathbf{u} = 0 \tag{2.1}$$

2. Conservation of momentum

$$\frac{\partial \mathbf{u}}{\partial t} + \mathbf{u} \cdot \bigtriangledown \mathbf{u} = -\frac{\bigtriangledown p}{\rho} + \frac{1}{\rho} \bigtriangledown \cdot (\mu(\bigtriangledown \mathbf{u} + \bigtriangledown^T \mathbf{u})) + \mathbf{g} + \frac{1}{\rho}\mathbf{T}_\sigma \tag{2.2}$$

Where $\mathbf{u}$ is velocity vector, p is the pressure, ρ is the density, μ is the viscosity, $\mathbf{g}$ is the gravity force and $\mathbf{T}_\sigma$ is the surface tension force.

As both fluids are considered to be incompressible, the continuity equation results in a divergence–free condition on the velocity field. The key difference in two–phase flow momentum equation compared to that of the single phase flow is the inclusion of the surface tension force term $\mathbf{T}_\sigma$. The surface tension force is a singular force acting only at the interface. This is given by Eq. 2.3,

$$\mathbf{T}_\sigma = \sigma\kappa\delta(\mathbf{x} - \mathbf{x}_f)\mathbf{n} \tag{2.3}$$

where $\mathbf{x}_f$ is the location of interface, $\mathbf{n}$ is the normal vector and σ is the surface tension coefficient. σ is modeled to be a constant value on the entire surface of the interface. In addition, a Kronecker delta function is introduced to make it physically consistent (acting only at the interface). The numerical code details and algorithms are presented in the following chapters.

2.2 Dynamic contact angles/lines

In this section, some relevant definitions and physics of the CAs are presented. The CA may be defined as the angle made by the interface at the wall, as shown in Fig. 2.1 for a 2D case. The CA is a multi–scale property and hence, there is a length scale involved when defining the same. For example, for an interface shown in Fig. 2.2, the CA made by the interface in the microscopic length scale (l_m) is different from that observed at a macroscopic length scale (L). The microscopic angle in general is denoted by θ_w and the macroscopic CA or the Apparent Contact Angle (ACA) is denoted by θ_{app}. Note that the CA observed experimentally is typically θ_{app}.

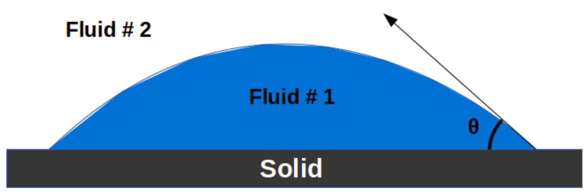

Figure 2.1: Contact angle definition

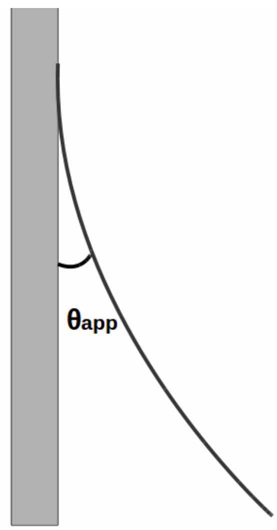

Figure 2.2: Apparent contact angle

If the interface is at rest relative to the wall boundary, θ_w is considered to be a Static Contact Angle (SCA) represented by θ_s. This angle depends on the material properties of the wall and the fluids in the system. Although θ_w is typically assumed to be constant ($= \theta_s$) for a given fluids and solid system, it was found that its value depends on the velocity of the interface (thus, Ca) as well (Blake and Haynes (1969)). This angle that the interface makes when it is in motion relative to the wall, is defined as the Dynamic Contact Angle (DCA), denoted by θ_d. θ_d depends on θ_s, Ca, macroscopic flow structure and also flow in the vicinity of the contact line (Shikhmurzaev (2006), Blake *et al.* (1999)).

For any numerical simulation involving contact lines, the CA is to be prescribed as a boundary condition at every time step. In case of macroscopic simulations, θ_{app} is prescribed instead of θ_w as a boundary condition, to obtain the correct macroscopic interface profile. There are different models available to calculate θ_{app}, of which the widely used models are presented in the following chapters.

Chapter 3

NUMERICAL METHODS

In this chapter, a brief overview of the numerical methods used in this study are presented. For the purpose of solving the Navier – Stokes equations presented in the Sec. 2.1, the CFD code NGA (Desjardins *et al.* (2008)) is used. For interface capturing and evaluating interfacial properties including curvature, the Level set Interface Tracking (LIT) code (Herrmann (2008)) is used.

3.1 Level set method for interface capturing.

There are two general approaches used to track the temporal evolution of the interface in multiphase flows; namely, explicit and implicit methods. In explicit methods, the interface is tracked explicitly, for instance, by tracking the marker points used to represent the interface (Hyman (1984)). On the other hand, in implicit methods, the interface is embedded in a scalar field and the entire scalar field is updated dynamically to capture the interface motion. The Level Set Method (LSM) is one of the implicit methods that can be used for this purpose.

The LSM for capturing evolving fronts was first introduced by Osher and Sethian (1988). In this method, the interface is embedded in a higher dimensional scalar level set field. At a given time, the interface shape and position are obtained implicitly through a constant level set (iso–surface) of a function used to represent the interface. Different functions can be used to represent an interface in LSM. For example, a signed distance function (Chopp (1993)) and a hyperbolic tangent function (Olsson and Kreiss (2005)) are widely used to represent the interface. In the current work, a signed distance function is used to represent the interface. Using this function, at any given point, the LS value (ϕ) is given by the shortest signed distance to the interface. This function also has the property given by Eq. 3.1. The sign of the ϕ value is used to differentiate between fluid zones in which the point lies. Hence the zero iso–surface of the LS field represents the interface.

$$|\bigtriangledown \phi| = 1 \tag{3.1}$$

Once the LS field is initialized using a signed distance function, the interface is transported implicitly by transporting the entire LS field. Since the transport of the interface in immiscible fluids involves only advection, the LS transport equation is given by Eq. 3.2 (scalar advection). Also, the interface is advected with the local flow velocities and hence the same are used in the advection equation. The required velocities are obtained from the flow solver at every time step. As can be observed, the advection equation is a Hamilton – Jacobi equation of hyperbolic nature. Hence, mathematically the information travels from the interface along the characteristics in a normal direction.

$$\frac{\partial \phi}{\partial t} + \mathbf{u}. \bigtriangledown \phi = 0 \tag{3.2}$$

Once the LS field is advected, the LS values at different points are not guaranteed to remain a signed distance function. While the simulation can still be continued, it is important to maintain a signed distance function property (Eq. 3.1) in order to maintain a constant thickness of the interface and for an accurate evaluation of curvature, as solving Eq. 3.2 could result in steep gradients in ϕ field (Sussman *et al.* (1994)). If there are errors in the curvature calculation, it leads to spurious currents near the interface (Herrmann (2008)). Hence the signed distance property is to be restored by reinitializing the LS field.

Various approaches were developed to reinitialize the LS field. One of the widely used methods and the one used in this work is Partial Differential Equation (PDE) based reinitialization, proposed by Sussman *et al.* (1994) given by Eq. 3.3. The key advantages of PDE based reinitialization over other methods are ease of parallelization and computational inexpensiveness. In this approach, at every time step, Eq. 3.3 is solved until reaching steady state in pseudo–time τ. To avoid moving the zero LS, a sign function can be used, which is given by Eq. 3.5. This is formulated such that the zero iso–surface ($\phi_0(\mathbf{x})$) remains the same before and after reinitialization. Also, a smoothed form of the sign function, as in Eq. 3.5 is used for numerical purpose of smoothing the jump discontinuity in the ρ or μ values across the interface, which results in an interface with finite thickness.

$$\frac{\partial \phi}{\partial \tau} = S(\phi_0)(1 - \sqrt{{\phi_x}^2 + {\phi_y}^2}) \tag{3.3}$$

$$\phi_0(\mathbf{x}) = \phi(\mathbf{x}, 0) \tag{3.4}$$

$$S_\epsilon(\phi_0) = \frac{\phi_0}{\sqrt{{\phi_0}^2 + \epsilon^2}} \tag{3.5}$$

Similar to the advection equation of LS field, Eq. 3.3 is a time evolution equation. Since this method relies on solving a PDE to steady state, numerical errors due to round–off, truncation or approximation are inevitable. This leads to change in ϕ values at the zero iso–surface which effectively move the interface and result in changes to the volumes of individual fluids. Hence to limit these errors, reinitialization is performed only when appropriate trigger conditions are met by the ϕ field. One way is to reinitialize only when the LS field diverges from being a distance function (3.1) as developed by Gómez *et al.* (2005). This is given by Eq. 3.6,

$$\max(|\bigtriangledown \phi|) > \alpha_{max} \quad or \quad \min(|\bigtriangledown \phi|) < \alpha_{min} \tag{3.6}$$

where α_{min} and α_{max} are real constants. In addition, the minimum and maximum number of pseudo iterations to be performed in each time step can also be used as a trigger.

3.2 Level Set Interface Tracking (LIT) code

The Level Set Interface Tracking (LIT) code uses a cell centered equidistant Cartesian grid and Finite Difference Method (FDM) to solve LS equations including advection and reinitialization. In addition, it also calculates other required quantities like curvature (κ). The code employs the Refined Level Set Grid (RLSG) method developed by Herrmann (2008). The key idea behind this approach is that an auxiliary equidistant Cartesian grid with higher resolution compared to the flow solver grid can be used to accurately define and track the interface motion. Thus interfaces which are highly curved can be represented more accurately compared to a standard LS approach, which helps in accurate calculation of curvature values. In order to achieve a grid with a manageable size, a two–level narrow band approach (Adalsteinsson and Sethian (1995) and Jiang and Peng (2000)) is used. In addition, for the LS advection and reinitialization, fifth–order WENO Scheme of Jiang and Peng (2000) coupled with TVD RK of third–order accuracy (Shu (1988)) are used for numerical stability.

3.3 Flow solver (NGA)

NGA is a finite–volume flow solver on a structured staggered mesh. It implements a second order conservative scheme for the spatial quantities as in Morinishi *et al.* (2004). For temporal quantities, second order integration is implemented as in Pierce (2001). It also has the balanced force algorithm (Francois *et al.* (2006)) implemented to reduce the spurious currents caused by curvature errors. Additional details about the flow solver can be found in Desjardins *et al.* (2008).

NGA uses Continuum Surface Force (CSF) model to calculate surface tension force in an explicit way and thus, imposes capillary time step limitation (Brackbill *et al.* (1992)). This limitation is in addition to the standard Courant – Friedrichs –

Lewy (CFL) condition for Navier – Stokes equations and is given by,

$$\triangle t \leq \triangle t_{cap} = \sqrt{\frac{(\rho_1 + \rho_2)\triangle^3}{4\pi\sigma}} \tag{3.7}$$

where $\triangle t$ is the time step, $\triangle t_{cap}$ is the capillary time – step, $\triangle$ is the characteristic grid size of the flow solver, ρ_1 and ρ_2 are the densities of the two fluids and σ is the surface tension coefficient.

3.4 Algorithm for solving a multiphase CFD problem

The NGA and LIT codes are coupled in order to simulate the time evolution of the interface. NGA requires the curvature (κ) from the LIT grid in order to evaluate the surface tension force ($\mathbf{T}_\sigma$). NGA also required the interface position to calculate the physical parameters including density and viscosity at a given point to calculate the flow variables. LIT obtains the velocities used for advection from NGA. The entire simulation process can be summarized using the following algorithm:

Algorithm 1 Solving multiphase CFD problem

Initialize the flow solver (velocities and pressure).

Set the BCs in the Flow Solver.

Initialize the level set field

while (time $\leq$ end time) **do**

  Advect the interface using velocities from flow solver.

  Reinitialize the LS Field

  Import interface position and curvature data into flow solver

  Advance the Flow Solver simulation by one time step

end while

Chapter 4

MATHEMATICAL MODELS FOR CONTACT ANGLES.

In this chapter, various mathematical models which are widely used in the literature to predict the Contact Angle (CA) made by the interface at the wall are presented.

4.1 Static Contact Angle (SCA) model.

One of the simplest CA models is for evaluating the SCA (θ_s, defined in 2.2) was developed by Young (1805) for a given solid – liquid – gas system. The model is given by Eq. 4.1,

$$\gamma_{sv} - \gamma_{sl} = \gamma_{lv} \cos\theta \tag{4.1}$$

where $\gamma_{sv}, \gamma_{sl}, \gamma_{lv}$ are the interfacial surface free energies for solid – vapor, solid – liquid and liquid – vapor pairs respectively. This equation is only valid for smooth surfaces and liquid – gas type of systems alone. Cassie and Baxter (1944) have developed a more accurate model considering the surface imperfections as well.

4.2 Hydrodynamic theory and dynamic contact angle models.

The multi–scale property of the CA is introduced in Sec 2.2, because of which, if one conducts an experiment to observe the CA in a multiphase system, it can be found that the observed apparent CA (θ_{app}) is not the same as the θ_w at microscopic level. Hence when performing numerical simulations, if a Direct Numerical Simulation (DNS) is performed (resolving all the length scales involved), θ_w itself is sufficient to obtain the right flow structure, without any further modeling of CA (Sui and Spelt (2013)). A DNS is many times not practical mainly because it is computationally very expensive and hence, θ_{app} needs to be modeled which is then used as a boundary condition. If modeled accurately, θ_{app} BC should result in a similar macroscopic interfacial structure as that of using θ_w as a boundary condition in a DNS.

There are currently two approaches to develop a DCA model for θ_{app}, Hydrodynamic Theory (HT) and the Molecular – Kinetic theory. A summary of both approaches can be found in Blake (2006). In the current research work, models based on HT are used. The key aspect of HT is that θ_{app} is primarily different from the θ_w because of viscous bending of the interface in the intermediate mesoscopic range (Blake (2006)). Thus, HT predicts that there are three regions in which the interface bending occurs, resulting in a length scale dependent CA ($\theta(r)$), as shown in Fig. 4.1. Here r is the distance from the point where θ is measured to the contact line. The length scales corresponding to the regions are microscopic (inner), mesoscopic (intermediate) and macroscopic (outer).

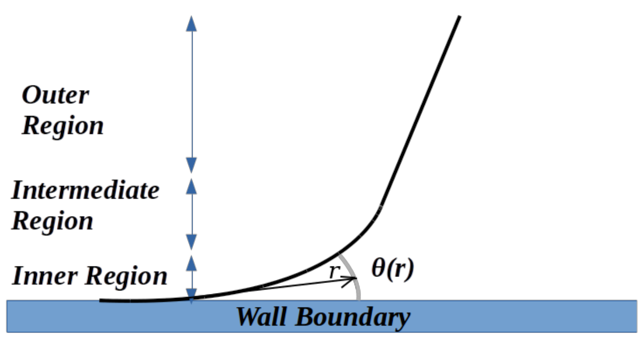

Figure 4.1: Viscous bending predicted by hydrodynamic theory.

4.2.1 HT and no–slip condition

One issue with classic HT is the incompatibility of the dynamic contact line with the standard no–slip BC used for solving the flow equations. As it is known, with the no–slip condition, the velocity of fluid or contact line on the wall is equal to that of the wall. Thus the no–slip condition on the wall leads to a non–integrable stress singularity at the contact line and thus the solution cannot be calculated near the contact line (Cox (1986)). One approach is to use a slip BC for velocity in the contact line region on the wall to relax the stress singularity and solve the problem.

A free–slip condition was proposed by Hocking (1977), for the contact line region (distance slip length (λ) around the contact line) and standard no–slip condition in the single phase region. This results in zero shear stress along the wall near the contact line and hence; allows for a solution to be calculated. Numerically, this implies setting the velocities in the ghost cells equal to that of the corresponding interior cells. Other approaches include making the shear stress finite and non–zero by implementing a slip BC developed by Navier (1823), as given by the Eq. 4.2,

$$u_{cl} - u_w = \lambda \frac{\partial u}{\partial y} \tag{4.2}$$

where u_{cl} is the velocity of the CL along the wall, u_w is the velocity of wall boundary, λ is the slip length and $(\frac{\partial u}{\partial y})$ is the shear stress component tangential to the wall. When $\lambda = 0$, it results in a $no - slip$ condition and when $\lambda = \infty$, it results in a free slip condition.

These slip models are easy to implement but are not accurate enough to capture the actual physics of contact line motion, as verified experimentally by Wilson *et al.* (2006). There are other recent slip models as well (Shikhmurzaev (2006)) which try to include the flow effects in the vicinity of the contact line.

4.2.2 Voinov model

The Voinov (1976) model is one of the earliest DCA models developed using HT, applicable for a liquid–gas system. The model was derived considering only the inner and outer regions of Fig. 4.1 and in the limit $Ca \to 0$, shown in Eq. 4.3,

$$\theta_{app}{}^3 - \theta_w{}^3 = 9Ca\ln(\frac{L}{l_m}) \tag{4.3}$$

where $\theta_{app} < \dfrac{3\pi}{4}$, L is the macroscopic length scale and l_m is the microscopic length scale. One of the main limitations of the model is that it is applicable to only systems with a liquid – gas interface, where the gas is assumed to be inviscid.

4.2.3 Cox model

Cox (1986) proposed a much more general and complete model for DCA compared to the existing models. His model is applicable to systems with two viscous fluids and was obtained considering three regions (as in Fig. 4.1.) similar to that of Hocking and Rivers (1982). The Navier slip law (Eq. 6.4.) was used to remove the stress singularity. The key idea of this theory is that, when three regions of expansion are considered, the solution in the intermediate region is independent of the inner and outer region solutions, when calculated to the lowest order of Ca. In case of next higher order of Ca, it was considered that the solution in intermediate region depends on only one constant from either the inner or outer regions. Once the solution is found for the intermediate region, it is then matched with the solutions in the inner and outer regions using asymptotic theories, leading to a general three region solution, given by Eq. 4.4, which is correct to O(Ca^2),

$$g(\theta_{app}) = [g(\theta_w) + Ca\ln(\epsilon^{-1})] + Ca[(f(\theta_w))^{-1}Q_i{}^* - (f(\theta_{app}))^{-1}Q_o{}^*] + O(Ca^2). \tag{4.4}$$

where

$$g(\theta) = \int_0^\theta \frac{d\theta}{f(\theta, \lambda)} \tag{4.5}$$

and

$$f(\theta, q) = \frac{2\sin\theta[q^2(\theta^2 - \sin^2\theta) + 2q[\theta(\pi-\theta) + \sin^2\theta] + (\pi-\theta)^2 - \sin^2\theta]}{q(\theta^2 - \sin^2\theta)[(\pi-\theta) + \sin\theta\cos\theta] + [(\pi-\theta)^2 - \sin^2\theta](\theta - \sin\theta\cos\theta)} \tag{4.6}$$

Here q is the ratio of viscosities between the two fluids, $\epsilon = \dfrac{\lambda}{L}$, λ is the slip length, L is the macroscopic length scale and Q_i^* and Q_o^* are constants based on the geometry of the interface in the inner and outer regions respectively. The Eq. 4.4 correct to O(Ca^0) is given by Eq. 4.7. This is currently the most widely used DCA model to obtain the BC for CA, in macroscopic numerical simulations.

$$g(\theta_{app}) = g(\theta_w) + Ca \ln(\epsilon^{-1}). \tag{4.7}$$

The key limitations of the Cox model are its validity in low Ca flows where surface tension force dominates the viscous force and in low Re flows where the inertial forces are negligible compared to the viscous forces. It is also assumed that the slip of the interface occurs within the slip length (λ) around the contact line and ϵ is assumed to be very small.

4.2.4 Mesh dependent DCA model by Afkhami et al. *(2009)*

In many numerical studies involving DCA and DCL, one of the key challenges is to obtain grid converging interface profiles. Afkhami *et al.* (2009) developed a DCA model which is specifically aimed at obtaining interface profiles which are consistent at a macroscopic length scale, obtained using different grid resolutions. The modified DCA model is given by Eq. 4.8,

$$g(\theta_{num}) = g(\theta_{app}) + Ca \ln(\frac{\triangle/2}{L}) \tag{4.8}$$

where θ_{num} is the CA boundary condition, $\triangle$ is the grid spacing and L is the macroscopic length scale. It is important to note that in this model, the θ_{num} is used as the boundary condition instead of θ_{app}, based on the grid spacing $\triangle$. Although a constant θ_{app} was used in this study, θ_{app} can be calculated using other DCA models separately. Hence for a given θ_{app}, this model can be used to obtain CA boundary condition (θ_{num}) which results in a grid converging macroscopic interface profile.

Chapter 5

PROPOSED METHOD FOR PRESCRIBING CONTACT ANGLE BC IN LEVEL SET METHOD.

In this chapter some of the approaches taken to apply the contact angle boundary condition and a simple approach to prescribe a given Contact Angle (CA) as the Boundary Condition (BC) in level set method (LSM) are presented.

5.1 Existing methods for prescribing CA boundary condition.

One of the earliest approaches in prescribing a CA boundary condition in a LSM formulation was developed by Sussman and Uto (1998) to study the spreading of a liquid drop. A static contact angle (θ_s) obtained from an experimental observation was used as the CA boundary condition. This CA boundary condition was implemented by a straight line (2D case) extension of the interface (ghost interface) from the contact line, with the required CA at the wall as shown in Fig. 5.1. The ghost interface is shown using a blue dashed line which makes the required CA θ_{app} with the wall. The LS ghost cell values (ϕ_g) are then set to signed distance to the ghost interfaces, wherever a normal can be drawn from the ghost interface to that cell, represented by blue shaded region. In the ghost cell zones where a normal from the interface cannot be drawn, represented by gray zone, extrapolated values for ϕ_g are used. This also involves identifying the contact points first by extrapolation of the interface to the wall. The approach was presented for a 2D problem. Also, a free slip condition was used at the contact line.

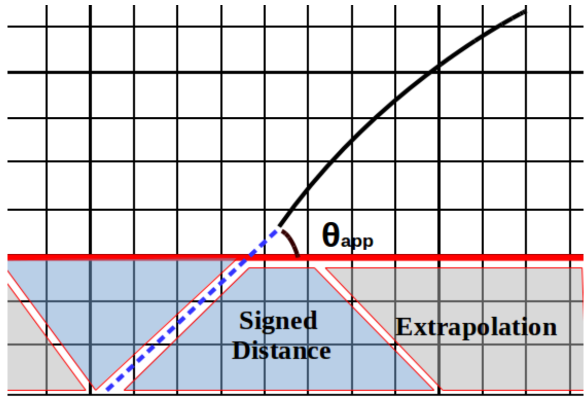

Figure 5.1: Straight line ghost interfaces to implement CA BC.

Spelt (2005) developed an approach to account for CA hysteresis and also for multiple contact lines. Although an approach similar to that of Sussman and Uto (1998) is followed to calculate ϕ_g, by using a straight–line extension of the interface (2D case), the key difference in this work is to prescribe the interface velocity rather than the CA. The CA model used is reformulated to calculate velocity as the boundary condition for the contact line. The required interface position and the CA value are determined iteratively.

Arienti and Sussman (2014) recently implemented the CA physics in a sharp interface approach with an embedded LS field by prescribing the normal at the contact line. Also, no − slip BC was used which numerically results in a grid dependent slip length for cell centered ϕ values. Recently Della Rocca and Blanquart (2014) developed a modified reinitialization equation to be applied specifically at the boundary adjacent LS cells (ϕ_w) in cases with contact lines in order to prescribe the CA boundary condition and to reduce the spurious currents resulting from curvature errors. Thus, instead of setting the ϕ_g values directly, their modified reinitialization equation reinitializes the LS field such that the CA BC is imposed at ϕ_w. In this study the free–slip BC was used at the wall with CL.

5.2 Proposed method for prescribing Contact Angles.

The effect of CA at the wall boundary is mainly important during the calculation of curvature and in the visualization of the interface shape at the wall at any given time step. The Neumann BC typically used for the ghost cell LS values (ϕ_g) always results in a 90^o contact angle which mostly results in an inaccurate curvature value and representation of the interface geometry at the boundary. Hence, the idea is to modify the ϕ_g values, such that the right contact angle is prescribed in ϕ_w cells. This should result in correct visualization of interface when plotted and also correct curvature values automatically.

Prescribing a CA in the ϕ_w cells is equivalent to prescribing a normal value at that point, as for a given CA value, there is a unique normal. The normal at a boundary cell ϕ_w can be calculated using (for a 2D problem),

$$\vec{N} = \frac{\bigtriangledown \phi}{|\bigtriangledown \phi|} \implies N_x = \frac{-\phi_x}{\sqrt{{\phi_x}^2 + {\phi_y}^2}}; N_y = \frac{-\phi_y}{\sqrt{{\phi_x}^2 + {\phi_y}^2}};$$
$$\phi_x = \frac{(\phi(i+1,j) - \phi(i-1,j))}{h_x}; \phi_y = \frac{(\phi(i,j+1) - \phi_g)}{h_y}; \quad (5.1)$$

where h_x and h_y are the grid spacings in x and y directions respectively. Eq. 5.1 is obtained using standard central differencing to calculate the normal components.

It is important to note that prescribing the normal should be done without altering the ϕ values inside the flow domain, so that the actual interface is not moved inadvertently and lead to volume change of individual fluids. Thus, the required normal can be prescribed by modifying the ϕ_g value in Eq. 5.1. If θ is the angle being prescribed for the interface shown in the Fig. 5.2, the target normal is given by Eq. 5.2.

$$N_{xtar} = -\cos(\frac{\pi}{2} - \theta) \quad ; \quad N_{ytar} = \sin(\frac{\pi}{2} - \theta) \qquad (5.2)$$

Thus, equating the ratios of target and current normal values and solving for ϕ_g,

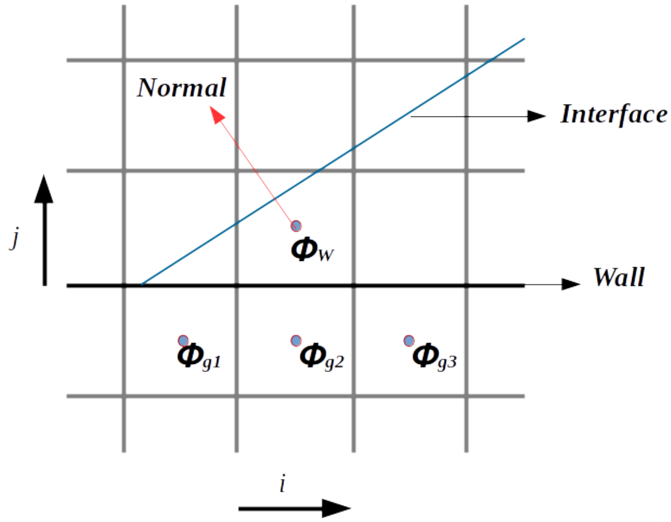

Figure 5.2: Wall boundary cell.

we obtain,

$$\phi_g = \phi(i, j+1) + \tan(\frac{\pi}{2} - \theta) \cdot \phi_x \cdot h_y \tag{5.3}$$

where h_y is the grid spacing in y–direction. Note that the Eq. 5.3 is valid only for a 2D case in which the interface is inclined as shown in Fig. 5.2. The expressions for other θ values can be derived in a similar way by calculating the target normal components and equating them to the standard normal formulas as in Eq. 5.1.

The curvature (κ) calculation in a LS formulation for a 3D problem is given by the Eq. 5.4.

$$\kappa = \frac{\phi_{,xx}(\phi_{,y}^2 + \phi_{,z}^2) + \phi_{,yy}(\phi_{,x}^2 + \phi_{,z}^2) + \phi_{,zz}(\phi_{,y}^2 + \phi_{,z}^2)}{(\phi_{,x}^2 + \phi_{y}^2 + \phi_{z}^2)^{3/2}} - 2\frac{\phi_{,xy}\phi_{,x}\phi_{,y} + \phi_{,xz}\phi_{,x}\phi_{,z} + \phi_{,yz}\phi_{,y}\phi_{,z}}{(\phi_{,x}^2 + \phi_{,y}^2 + \phi_{,z}^2)} \tag{5.4}$$

κ calculation in any cell using Eq. 5.4 involves a 27 point stencil of ϕ cells (9 in a 2D problem), when standard central differencing is used. Note that κ calculated using this formula at any point is the κ of the iso – surface which passes through

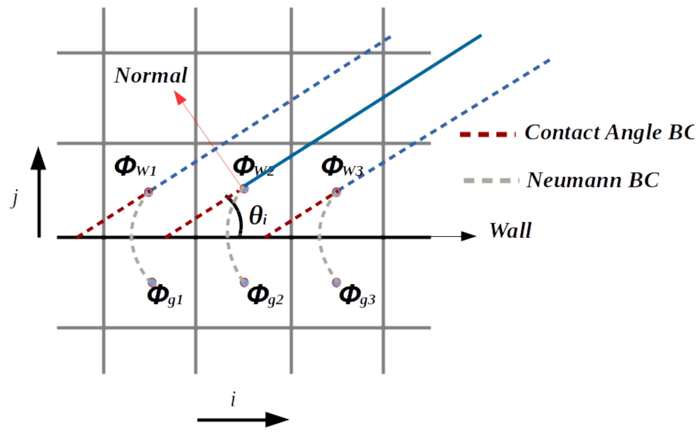

Figure 5.3: Curvature calculation in wall adjacent cell.

the point itself and not that of the actual interface (zero iso–surface). Now consider κ calculation in ϕ_{w2} cell as shown in the Fig. 5.3, for a planar interface. In this example, the CA of the iso–surface through ϕ_{w2} is assumed to be the same as that of the prescribed CA. Hence this should result in a $\kappa_{w2} = 0$. For this to be true, the iso–urface through ϕ_{w1}, ϕ_{w2} and ϕ_{w3} needs to have the same curvature. Hence the same CA BC should be applied to calculate ϕ_{g1} and ϕ_{g3} in addition to ϕ_{g2}, in order to avoid curvature errors.

The key difference between this method and the ones proposed earlier in LS approach is that the ϕ values are not strictly signed distance functions but are obtained such that the required normal is imposed at the boundary cells. Hence it can be considered as prescribing a normal rather than ϕ values directly.

Note that the angle being prescribed could be a SCA (same in every time step) or a DCA (varies every time step), but the approach to setting the CA BC remains the same. Only difference being, when prescribing a DCA, the value is calculated at every time step of the simulation using any of the previously described models.

5.3 Extension to 3D problems.

The definition of a contact angle for a 3D interface is not as straight forward as in a 2D case. In a 3D domain, the contact angle can be defined as the angle between the tangential surface of the interface and the wall. By this definition, only the z component of the target normal is varied when CA BC is changed and the x and y components remain the same, as shown in Fig. 5.5. The rest of the procedure remains the same in obtaining the ϕ_g value (in z direction in this example).

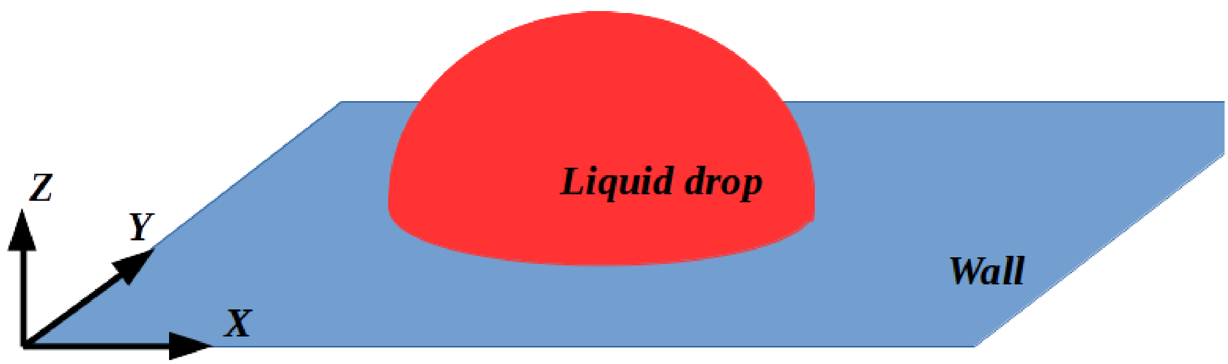

Figure 5.4: 3D drop on a Wall.

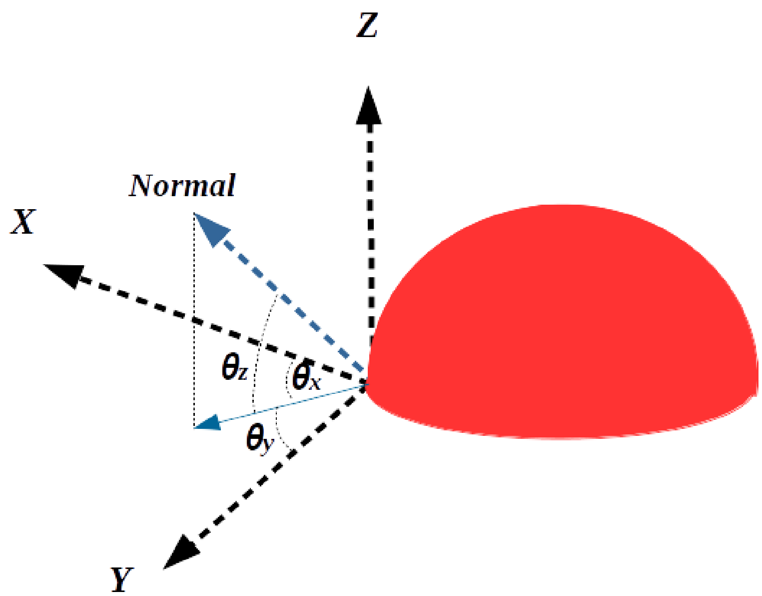

Figure 5.5: Contact angle calculation in 3D.

5.4 Results and observations

In order to test the proposed approach, a simple 2D test case is presented as shown in Fig. 5.6. A planar interface which is initially horizontal is considered with initial contact angles being 90^0 on both left and right walls. Now different CA boundary conditions are prescribed on opposite walls such that the sum of both the angles is 180^0 (in order to obtain a straight line steady state profile). The smallest or largest angle that can be prescribed in this case depends on the size of the domain. The true solution is a static straight line with its contact angle values equal to the ones prescribed in the boundary conditions, as there is no other external or body forces acting on the system.

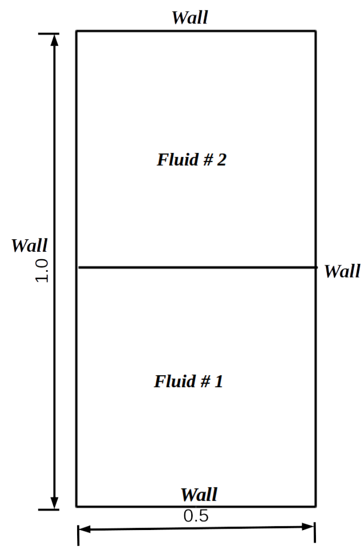

Figure 5.6: Test case for prescribing SCA.

The physical values used for the fluid system are the same as the ones considered in Afkhami *et al.* (2009). Both the fluids are chosen to have same densities and viscosities of 1.0 and 0.25 respectively. Surface tension constant σ is set to 7.5. Also, the gravitational force is not considered in this problem. These values are chosen such that the resulting flow has low Re and low Ca. There are two reasons why these regimes are chosen: to avoid any inertial effects and also to maximize the effect of surface tension force on the system. The results and comparison with the true solution is shown in Fig. 5.7.

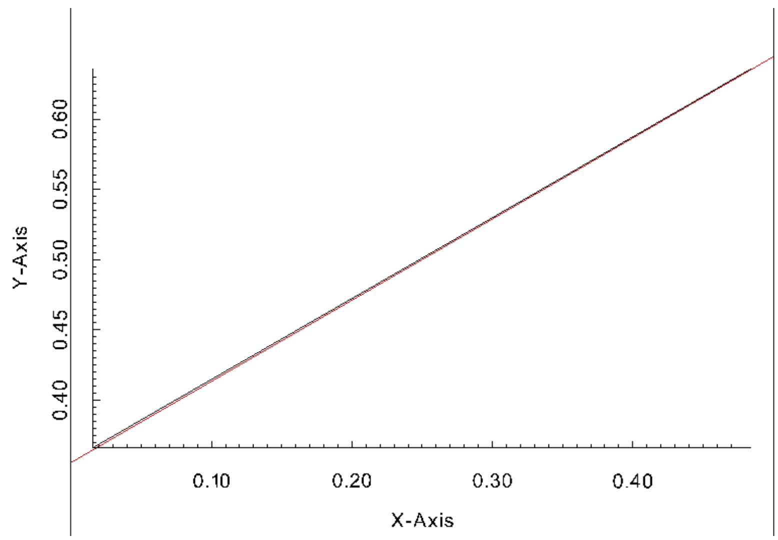

(a) $\theta_{left} = 120^o, \theta_{right} = 60^o$

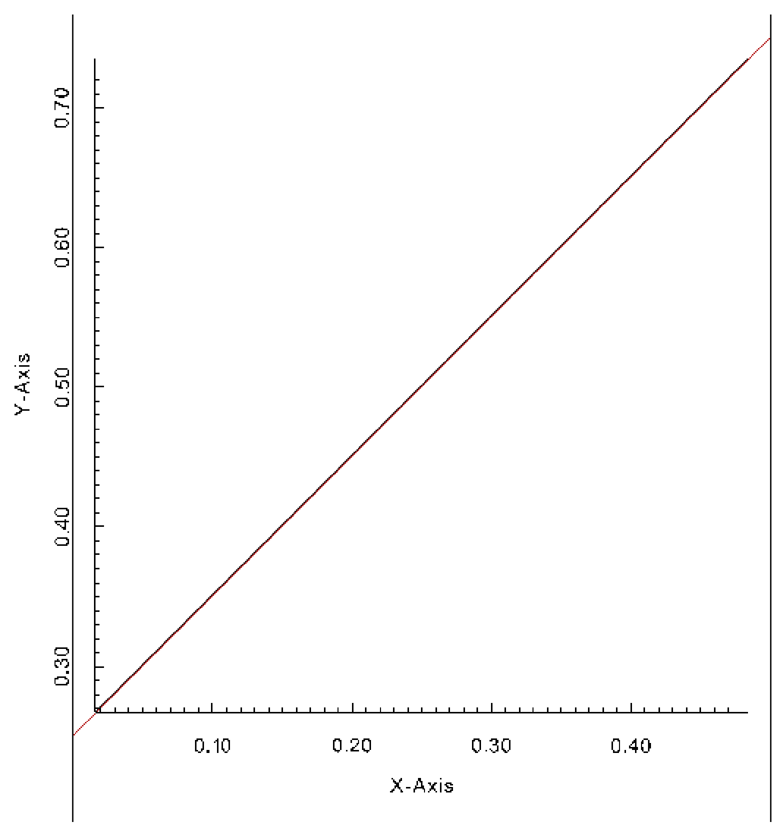

(b) $\theta_{left} = 135^o, \theta_{right} = 45^o$

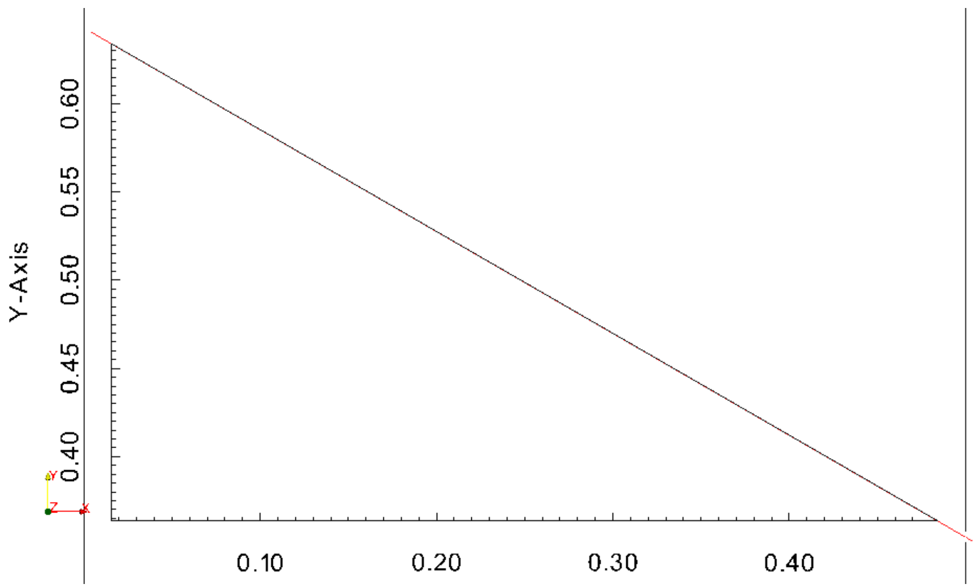

(c) $\theta_{left} = 60^o, \theta_{right} = 120^o$

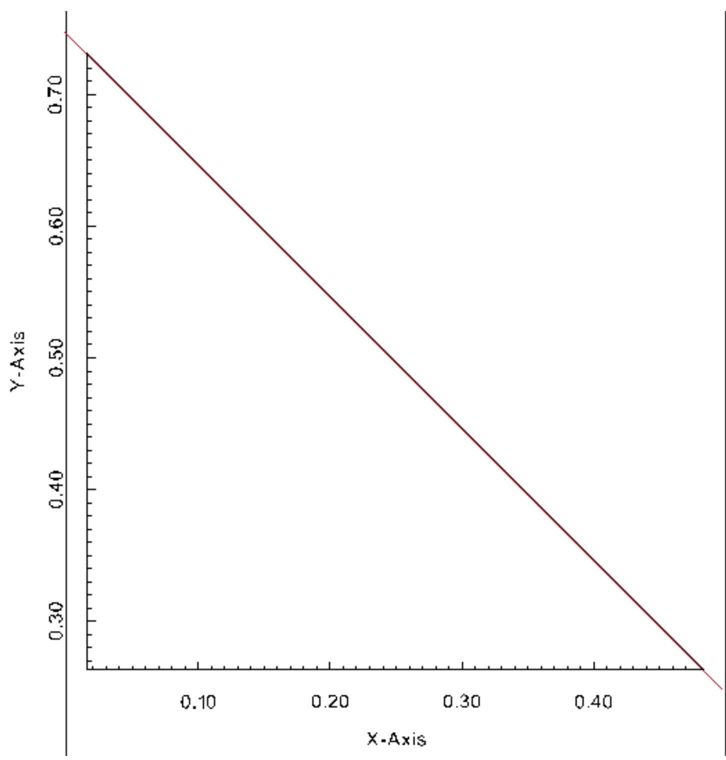

(d) $\theta_{left} = 45^o, \theta_{right} = 135^o$

Figure 5.7: Planar interface test for prescribing static contact angle.

The red line in each plot represents the theoretical steady state solution and the black line represents the solution obtained using the current method for prescribing the CA. From the above results it can observed that the steady state profile is visually very well aligned with the theoretical solution. In this case, at every time step a constant SCA value is prescribed. The temporal evolution of the interface shape for the case with $\theta_{left} = 60^0$ and $\theta_{right} = 120^0$ is shown in the Fig. 5.8.

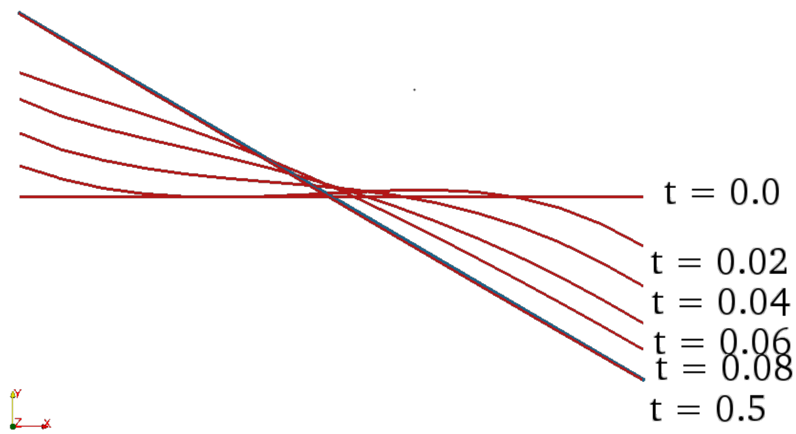

Figure 5.8: Temporal evolution of the interface shape with $\theta_{left} = 60^0, \theta_{right} = 120^0$.

It is important to note that when a contact angle value very different from the current or local CA value is prescribed, a very high curvature and thus surface tension force is applied at the contact line suddenly. This could lead to break–up of the interface at the wall.

A simple test case which can be used to test the SCA BC prescription numerically is to initialize the LS field with BCs on ϕ such that the interface has a CA value equal to the prescribed SCA value. This should result in zero curvature and thus no contact line motion, if no other forces including gravity are acting. Fig. 5.9 shows such configurations in the current approach and the corresponding curvature values initially obtained.

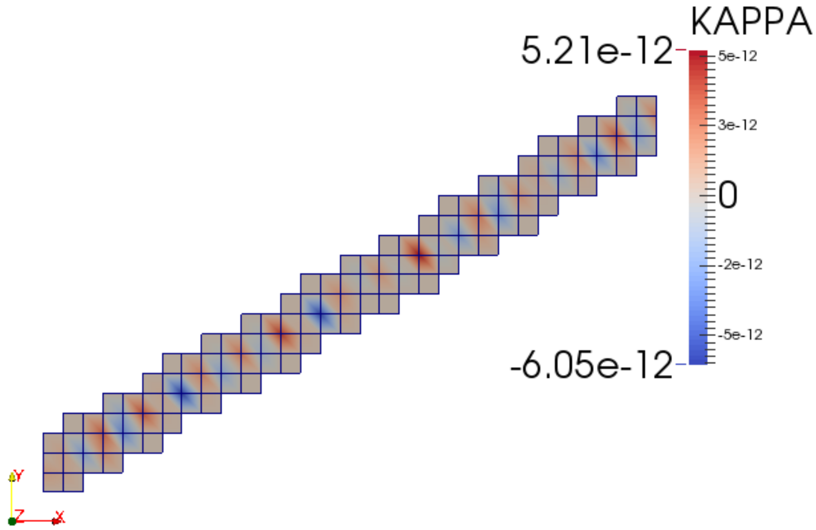

(a) $\theta_{left} = 120^o, \theta_{right} = 60^o$

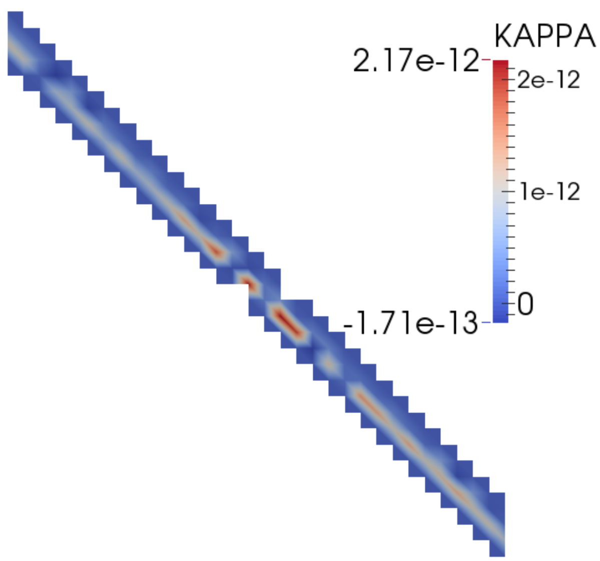

(b) $\theta_{left} = 45^o, \theta_{right} = 135^o$

Figure 5.9: Initial curvature values for straight line interfaces

Chapter 6

GRID CONVERGENCE OF INTERFACE PROFILES

In the previous chapters, the procedure to implement a given contact angle value at any time step during the simulation is presented and the approach is tested by prescribing a fixed SCA value. In real applications, this value becomes a boundary condition which is obtained from a Dynamic Contact Angle (DCA) model. Some of the models are discussed in the Ch. 4. In addition to the implemention of a DCA model, there are a few issues with moving Contact Lines (CL) which are to be addressed. The first one being the effects of reinitialization of the level set (LS) field on CA implementation and the second being handling the stress singularity at the moving CL. These issues are addressed in this chapter and then implementation of a DCA model is discussed.

6.1 Effects of reinitialization on CA implementation

As it is known, the LS method is not volume conserving by nature, partly because of reinitialization of the LS field. By solving the reinitialization equation (Eq. 3.3), the ϕ values inside the domain are modified such that the distance function property (Eq. 6.1) is restored. Although the reinitialization equation is formulated to not move the zero iso–surface, in practice it does move the interface and thus results in volume change of individual fluids. This is more pronounced in the regions with high gradients in the ϕ values, which are inevitable when incorporating the CA BC. Thus reinitialization is triggered more often when the contact angle value at a given time step is very different from the prescribed CA BC, as also noted by Della Rocca and Blanquart (2014), resulting in volume change of individual fluid zones.

In order to test the effects of reinitialization on prescribing a CA, the test case presented in Sec. 5.4 is solved with different reinitialization trigger conditions. The same physical properties of fluids, with CA BCs of $\theta_{left} = 60^0$ and $\theta_{right} = 120^0$ are used and solved until the interface reaches a steady state, on a grid of size 16 X 32. The trigger conditions used are given by Eq. 3.6. The trigger values used are, for the low reinitialization case $\alpha_{min} = 1e-4$ and $\alpha_{max} = 2.0$; for the intermediate reinitialization $\alpha_{min} = 0.1$ and $\alpha_{max} = 1.8$; and for the high reinitialization case $\alpha_{min} = 0.5$ and $\alpha_{max} = 1.5$. Fig. 6.1 shows the steady state profile obtained with different reinitialization trigger parameters and also the change in volume with time in corresponding settings. The volume change observed with low reinitialization = 0.0484%, intermediate reinitialization = 1.060% and with high reinitialization = 0.944%.

$$|\bigtriangledown \phi| = 1 \tag{6.1}$$

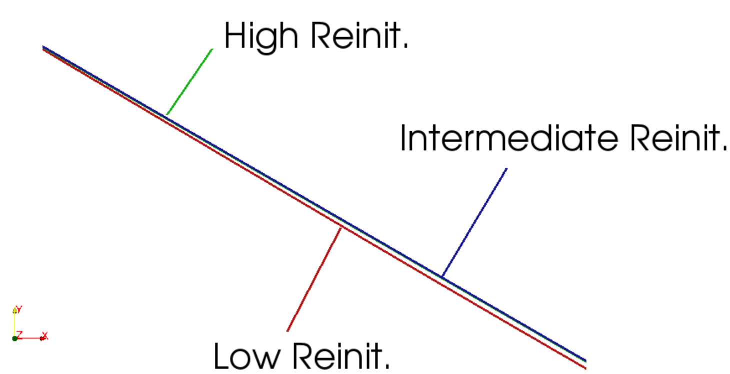

(a) Steady state interface profile with varying reinitialization triggers

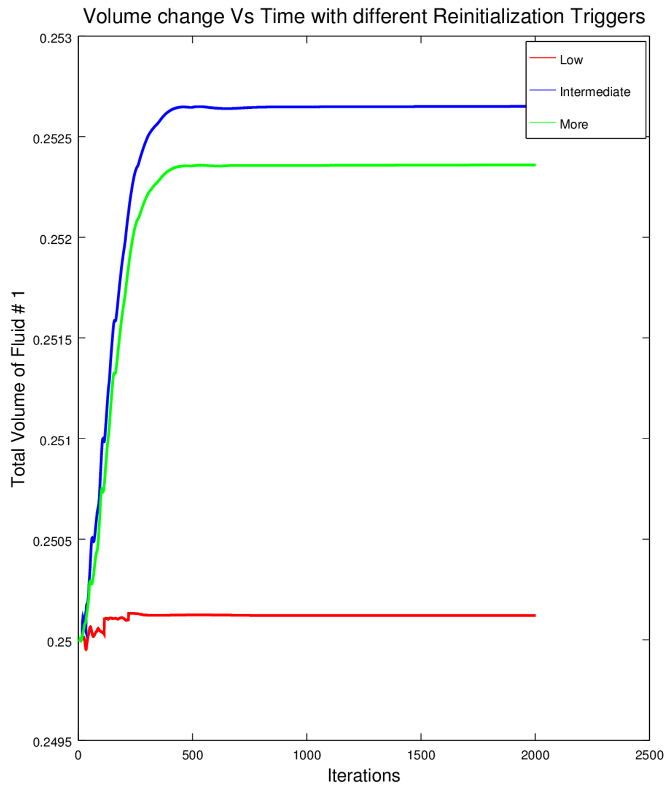

(b) Volume change in time with varying reinitialization triggers.

Figure 6.1: Effect of reinitialization on steady state profile.

It should be noted that neither the current approach to set the normals nor the standard Neumann BC necessarily result in ϕ_g values which satisfy Eq. 6.1. But Neumann BC (zero - gradient) results in smoother ϕ values than setting the normals. Hence, the proposed approach might trigger the reinitialization procedure more often than the Neumann BC resulting in volume loss. This can be reduced by making a small change to the algorithm of advection and reinitialization of ϕ field; by first calculating ϕ_g using the Eq. 6.1 or using Neumann and then setting the CA boundary conditions.

Algorithm 2 Reducing volume change due to reinitialization

Advect the ϕ values.

Set the ϕ_g values using Eq.6.1 or Neumann BC.

Reinitialize the Level Set Field

Set ϕ_g values using CA BC.

By making this change, unnecessary reinitialization triggered by the CA BC can be avoided and a reduction in volume errors can be obtained. This approach is similar to the modification of te reinitialization equation proposed by Della Rocca and Blanquart (2014). The difference being, instead of modifying the reinitialization equation, the ϕ_g values are adjusted directly to reduce the reinitialization effect at the boundary adjacent cells. In the current study, reinitialization is performed every time step without exceeding 5 pseudo reinitialization time steps in addition to setting the trigger conditions of $\alpha_{min} = 1e - 4$ and $\alpha_{max} = 2.0$ as in Eq. 3.6.

6.2 Stress singularity at contact line

One of the key requirements in the implementation of a DCA model is the grid convergence of interface profile. Although there are many prior studies involving implementation of DCA in LS and Volume of Fluid (VoF) approaches, only recently efforts have been made (first by Afkhami *et al.* (2009)) to address the issue of grid convergence of the interface profile. It was observed that when a standard no–slip condition is used, it leads to the divergence of the wall shear stress component and the interface profile at steady state; at increasing levels of grid refinement (Afkhami *et al.* (2009),Sui and Spelt (2013),Shikhmurzaev (2006)).

To test the convergence of the interface profile at steady state with LIT and NGA, a test case similar to that of the one used in Afkhami *et al.* (2009), as in Fig. 6.2

is used. The 2D domain consists of walls on all boundaries. The left wall is moving in the $+y$ direction with a velocity $u_w = 1.0$ inducing shear into the system. The interface initially has a CA of 90^0 and different CA values can be prescribed as a BC, as discussed in Ch. 5. Since this test case is aimed at testing grid convergence of interface profile at steady state, only SCA values are prescribed. Also, gravity is not considered as it reduces the overall height to which the interface rises.

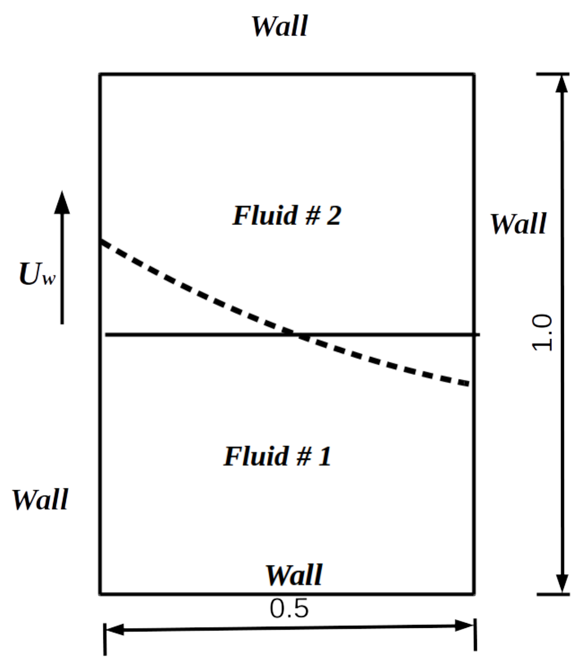

Figure 6.2: Test case: Moving contact line in a shear induced flow.

On the right wall, a free–slip condition with a Neumann BC for ϕ is applied. First, the standard Neumann BC on ϕ which implies a 90^o contact angle at the wall is tested for grid convergence of contact line height (Fig. (6.3)). The overall mass change in each set up was found to be less than 1%.

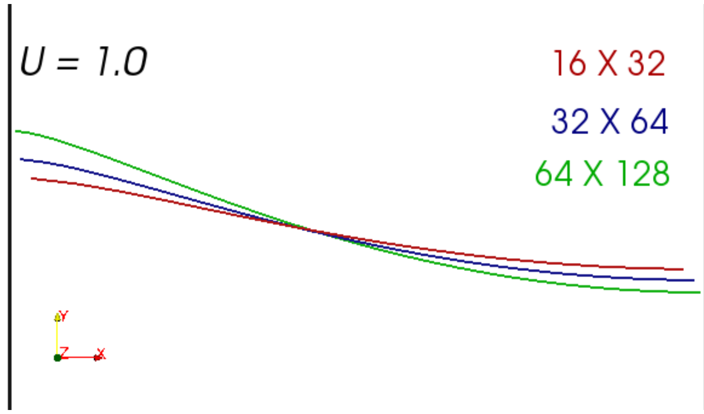

Figure 6.3: Divergence of contact line height with no – slip condition.

From Fig. 6.3 it can be observed that the contact line does not converge with the standard no–slip BC. The divergence of contact line height is mainly because the shear stress component along the wall does not converge with grid refinement due to the no–slip condition. This is the standard BC at walls while solving Navier – Stokes equations in single phase problems. Numerically, in a staggered grid setup, this condition is implemented using the ghost cell velocity components as there is no tangential velocity component calculated on the wall in the standard staggered grid approach. Thus, by extrapolation, the ghost cell velocity v_g is given by Eq. 6.2,

$$U_w = \frac{v_i + v_g}{2} \implies v_g = -v_i + 2U_{wall} \tag{6.2}$$

where U_{wall} is the velocity of the wall, v_g is the ghost cell velocity and v_i is the interior wall adjacent cell velocity. The corresponding shear stress component tangential to the wall can be calculated as in Eq. 6.3,

$$\tau_w \approx \frac{\partial v}{\partial x} \implies \tau_{wall} \approx \frac{v_i - v_g}{\triangle} \tag{6.3}$$

where τ_w is the wall shear stress component and $\triangle$ is the grid spacing. At steady state, v_i goes to zero. Which implies, with grid refinement, τ_w increases continuously without converging to a finite value. Note that the contact line moves because of the implicit slip ($\frac{\triangle}{2}$) offered by the staggered velocities and cell centered ϕ velocities which are advected. This corresponds to a slip –length of $\frac{\triangle}{2}$, which is obviously grid dependent. Hence it can be expected that the contact line height does not converge with standard no–slip condition.

6.3 Grid convergence using slip boundary condition

One approach to handle this stress singularity and remove the implicit slip length dependence is to use a slip BC with a slip length λ as in Eq. 6.4, as proposed by Navier (1823). This BC can be implemented using Eq. 6.5 (Afkhami *et al.* (2009)).

$$u - u_w - = \lambda(\frac{\partial u}{\partial x}) \tag{6.4}$$

$$u_g = \frac{2u_w \triangle - (\triangle - 2\lambda)v_i}{\triangle + 2\lambda} \tag{6.5}$$

Using this value for u_g, as opposed to the one derived in Eq. 6.2, reduces the shear stress singularity and must result in a grid converging interface profile. This can be verified by evaluating τ_w as in Sec. 6.2. Thus using the u_g value from the slip condition, the new τ_w value at steady state can be estimated as in Eq. 6.6. From this relation it can be observed that as grid refinement increases ($\triangle \to 0$), the wall shear stress τ_w converges to a constant value depending on the value of λ.

$$(\tau_w)_{steady} \approx \frac{-2u_w}{\triangle + 2\lambda} \tag{6.6}$$

It was observed that the slip happens at a length scale of 10–1000 nm (Cox (1986), Spelt (2005), Sui *et al.* (2014)). Numerically, this implies that the Navier slip condition is to be applied around the contact line within the slip length. This requires the grid size to be chosen such that the slip length is fully resolved, which is computationally expensive. It was observed by Dupont and Legendre (2010) that even when slip –length (λ) was chosen to be significantly larger than the nanometer scale, as long as the grid size is chosen such that λ is fully resolved, their results were found to be close to the experimental results. Using this approach to prescribe a macroscopic slip length, it was observed that the results with different grid resolution are very close to each other. First, just the slip model ($\lambda \approx 4\triangle_{32}$) is implemented without applying any contact angle. Next a 60^o constant contact angle is applied with slip values of $0.1(\lambda \approx 4\triangle_{32})$ and 0.06 ($\lambda \approx 2\triangle_{32}$).

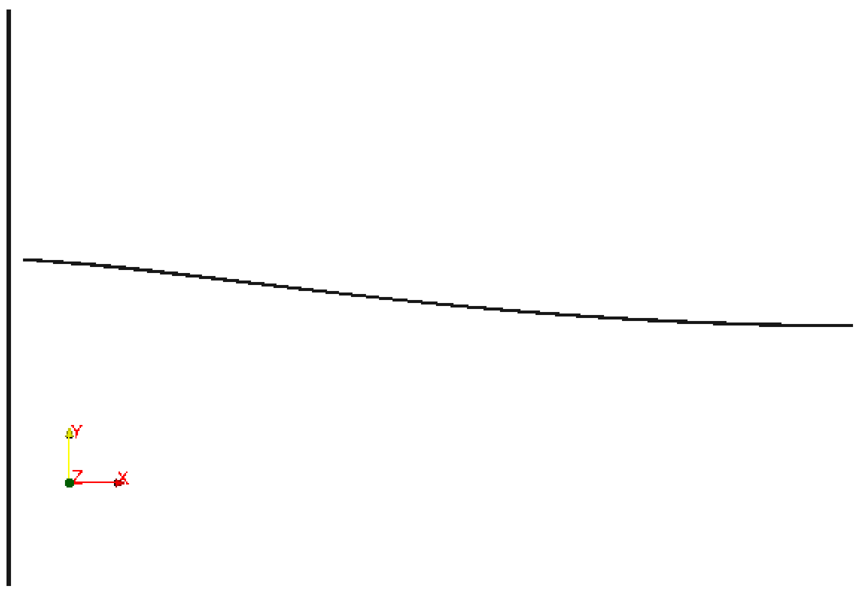

(a) $\theta_s = 90^o$, $\lambda = 0.1$ (Grid Sizes: 16 X 32, 32 X 64, 64 X 128, 128 X 256)

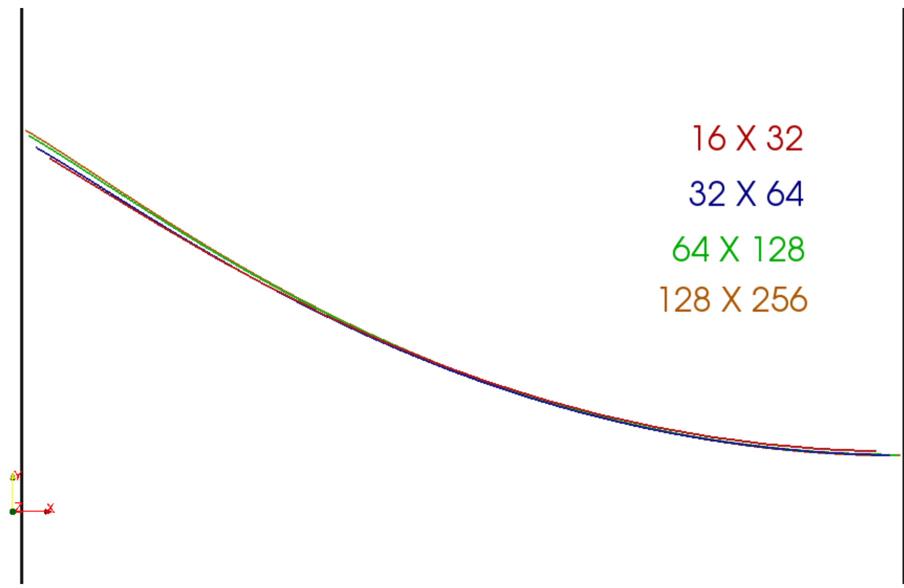

(b) $\theta_s = 60^o$, $\lambda = 0.1$

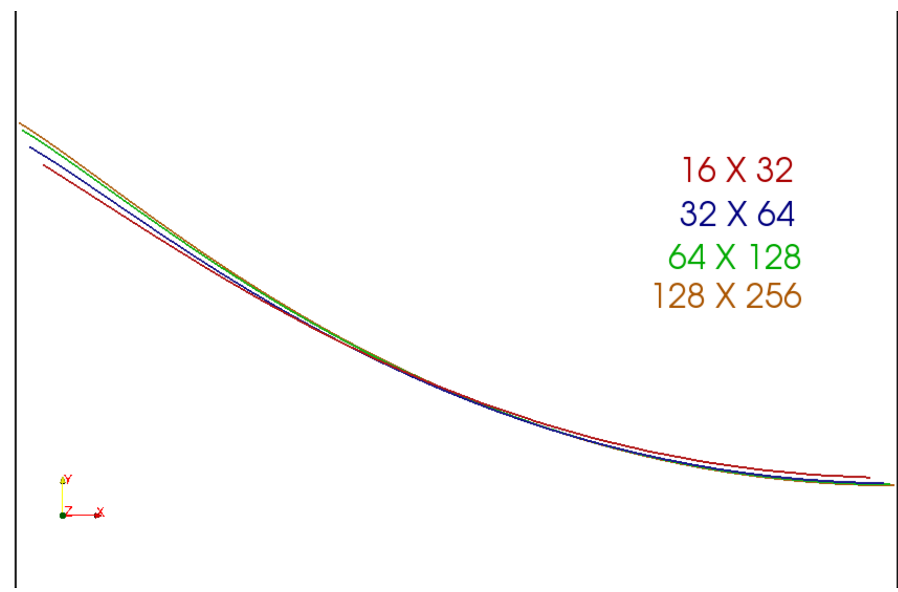

(c) $\theta_s = 60^o$, $\lambda = 0.06$

Figure 6.4: Grid convergence of contact line height with slip model

6.4 Implementation of dynamic contact angle model

Some of the widely used Dynamic Contact Angle models available in the literature were introduced in Ch. 4. Most of these models are only valid in the low Re and low Ca flows. Very limited research has been done to develop a DCA model valid for inertial (high Re) flows. Hence only the existing, widely used DCA model developed by Cox (1986) using Hydrodynamic theory is implemented in the codes (LIT and NGA). Note that the important equations related to the implemented DCA model from Ch. 4 are restated. The equations solved in this model are,

$$g(\theta_{app}) = g(\theta_w) + Ca \ln(\epsilon^{-1}). \tag{6.7}$$

where θ_w is the microscopic contact angle value which is input parameter and $\epsilon = \frac{\lambda}{L} << 1$. $g(\theta)$ is given by

$$g(\theta) = \int_0^\theta \frac{d\theta}{f(\theta, \lambda)} \tag{6.8}$$

$$f(\theta, q) = \frac{2\sin\theta[q^2(\theta^2 - \sin^2\theta) + 2q[\theta(\pi - \theta) + \sin^2\theta] + (\pi - \theta)^2 - \sin^2\theta]}{q(\theta^2 - \sin^2\theta)[(\pi - \theta) + \sin\theta\cos\theta] + [(\pi - \theta)^2 - \sin^2\theta](\theta - \sin\theta\cos\theta)} \tag{6.9}$$

In the above equations, q is the ratio of viscosities. As mentioned earlier, Eq. 6.7 is a lower order equation. Higher order terms can be derived based on other parameters including geometry of the flow (Sui and Spelt (2013)). Eq. 6.7 is solved using any standard non–linear solving method. Eq. 6.8 is solved using standard numerical integration techniques.

Chapter 7

CONCLUSIONS

First, a simple method to prescribe a given Contact Angle (CA) was implemented which can be easily extended to 3D. This approach guarantees that the correct CA boundary conditions are applied by prescribing the normals and thus generates correct curvature values which are very important in reducing the spurious currents. This approach is tested using simple test cases which are not computationally expensive and the results were found to be in agreement with the theoretical solutions.

One of the key problems identified with the CA implementation is the grid convergence of the interface profile in shear induced flows. The reasons for the divergence of interface profile were explored. It was concluded that the divergence of wall shear stress component at steady state with grid refinement is the reason for the divergence of the contact line height. Navier slip boundary condition was implemented to remove the stress singularity. Using a simple test case in 2D, it was found that in order to obtain grid converging interface profiles, the slip–length must be fully resolved.

Other numerical issues including the effects of reinitialization on CA BC were presented. Finally various dynamic contact angle models available in the literature were discussed and the widely used models of Cox (1986) and Voinov (1976) were implemented in LIT and NGA.

7.1 Future work

In this work, the slip model used was based on the experimental observations of Dupont and Legendre (2010). The physical validity of the Navier slip model for different test cases needs to be tested. There are currently slip models which are developed based on more realistic assumptions Shikhmurzaev (2006), which can be used. The reinitialization routine can be modified similar to the work of Della Rocca and Blanquart (2014), to assist setting the CAs, resulting in better volume conservation of individual fluids and thus improving the accuracy.

REFERENCES

Adalsteinsson, D. and J. A. Sethian, “A fast level set method for propagating interfaces”, Journal of computational physics **118**, 2, 269–277 (1995).

Afkhami, S., S. Zaleski and M. Bussmann, “A mesh-dependent model for applying dynamic contact angles to vof simulations”, Journal of Computational Physics **228**, 15, 5370–5389 (2009).

Arienti, M. and M. Sussman, “An embedded level set method for sharp-interface multiphase simulations of diesel injectors”, International Journal of Multiphase Flow **59**, 1–14 (2014).

Blake, T., M. Bracke and Y. Shikhmurzaev, “Experimental evidence of nonlocal hydrodynamic influence on the dynamic contact angle”, Physics of Fluids (1994-present) **11**, 8, 1995–2007 (1999).

Blake, T. and J. Haynes, “Kinetics of liquidliquid displacement”, Journal of colloid and interface science **30**, 3, 421–423 (1969).

Blake, T. D., “The physics of moving wetting lines”, Journal of Colloid and Interface Science **299**, 1, 1–13 (2006).

Brackbill, J., D. B. Kothe and C. Zemach, “A continuum method for modeling surface tension”, Journal of computational physics **100**, 2, 335–354 (1992).

Cassie, A. and S. Baxter, “Wettability of porous surfaces”, Transactions of the Faraday Society **40**, 546–551 (1944).

Chopp, D. L., “Computing minimal surfaces via level set curvature flow”, Journal of Computational Physics **106**, 1, 77–91 (1993).

Cox, R., “The dynamics of the spreading of liquids on a solid surface. part 1. viscous flow”, Journal of Fluid Mechanics **168**, 169–194 (1986).

Della Rocca, G. and G. Blanquart, “Level set reinitialization at a contact line”, Journal of Computational Physics **265**, 34–49 (2014).

Desjardins, O., G. Blanquart, G. Balarac and H. Pitsch, “High order conservative finite difference scheme for variable density low mach number turbulent flows”, Journal of Computational Physics **227**, 15, 7125–7159 (2008).

Dupont, J.-B. and D. Legendre, “Numerical simulation of static and sliding drop with contact angle hysteresis”, Journal of Computational Physics **229**, 7, 2453–2478 (2010).

Francois, M. M., S. J. Cummins, E. D. Dendy, D. B. Kothe, J. M. Sicilian and M. W. Williams, “A balanced-force algorithm for continuous and sharp interfacial surface tension models within a volume tracking framework”, Journal of Computational Physics **213**, 1, 141–173 (2006).

Gómez, P., J. Hernandez and J. López, "On the reinitialization procedure in a narrow-band locally refined level set method for interfacial flows", International Journal for Numerical Methods in Engineering **63**, 10, 1478–1512 (2005).

Herrmann, M., "A balanced force refined level set grid method for two-phase flows on unstructured flow solver grids", Journal of Computational Physics **227**, 4, 2674–2706 (2008).

Hocking, L., "A moving fluid interface. part 2. the removal of the force singularity by a slip flow", J. Fluid Mech **79**, 2, 209–229 (1977).

Hocking, L. and A. Rivers, "The spreading of a drop by capillary action", Journal of Fluid Mechanics **121**, 425–442 (1982).

Huh, C. and S. Mason, "The steady movement of a liquid meniscus in a capillary tube", Journal of fluid mechanics **81**, 03, 401–419 (1977).

Hyman, J. M., "Numerical methods for tracking interfaces", Physica D: Nonlinear Phenomena **12**, 1, 396–407 (1984).

Jiang, G.-S. and D. Peng, "Weighted eno schemes for hamilton–jacobi equations", SIAM Journal on Scientific computing **21**, 6, 2126–2143 (2000).

Morinishi, Y., O. V. Vasilyev and T. Ogi, "Fully conservative finite difference scheme in cylindrical coordinates for incompressible flow simulations", Journal of Computational Physics **197**, 2, 686–710 (2004).

Navier, C., "Mémoire sur les lois du mouvement des fluides", Mémoires de lAcadémie Royale des Sciences de lInstitut de France **6**, 389–440 (1823).

Olsson, E. and G. Kreiss, "A conservative level set method for two phase flow", Journal of computational physics **210**, 1, 225–246 (2005).

Osher, S. and J. A. Sethian, "Fronts propagating with curvature-dependent speed: algorithms based on hamilton-jacobi formulations", Journal of computational physics **79**, 1, 12–49 (1988).

Pierce, C. D., *Progress-variable approach for large-eddy simulation of turbulent combustion*, Ph.D. thesis, Citeseer (2001).

Shikhmurzaev, Y. D., "Singularities at the moving contact line. mathematical, physical and computational aspects", Physica D: Nonlinear Phenomena **217**, 2, 121–133 (2006).

Shu, C.-W., "Total-variation-diminishing time discretizations", SIAM Journal on Scientific and Statistical Computing **9**, 6, 1073–1084 (1988).

Spelt, P. D., "A level-set approach for simulations of flows with multiple moving contact lines with hysteresis", Journal of Computational Physics **207**, 2, 389–404 (2005).

Sui, Y., H. Ding and P. D. Spelt, “Numerical simulations of flows with moving contact lines”, Annual Review of Fluid Mechanics **46**, 97–119 (2014).

Sui, Y. and P. D. Spelt, “An efficient computational model for macroscale simulations of moving contact lines”, Journal of Computational Physics **242**, 37–52 (2013).

Sussman, M., P. Smereka and S. Osher, “A level set approach for computing solutions to incompressible two-phase flow”, Journal of Computational physics **114**, 1, 146–159 (1994).

Sussman, M. and S. Uto, “A computational study of the spreading of oil underneath a sheet of ice”, CAM Report **114**, 146–159 (1998).

Voinov, O., “Hydrodynamics of wetting”, Fluid Dynamics **11**, 5, 714–721 (1976).

Walpot, R., F. Ganzevles and C. Van der Geld, “Effects of contact angle on condensate topology, drainage and efficiency of a condenser with minichannels”, Experimental thermal and fluid science **31**, 8, 1033–1042 (2007).

Wilson, M. C., J. L. Summers, Y. D. Shikhmurzaev, A. Clarke and T. D. Blake, “Nonlocal hydrodynamic influence on the dynamic contact angle: Slip models versus experiment”, Physical Review E **73**, 4, 041606 (2006).

Young, T., “An essay on the cohesion of fluids”, Philosophical Transactions of the Royal Society of London pp. 65–87 (1805).